Inhibiting histone acetylation in CREBBP/EP300 mutants leads to synthetic cytotoxicity via repression of homologous recombination.

Manish Kumar PhD[1]*, David Molkentine BS[2]*, Jessica Molkentine BS[2], Kathleen Bridges MS[1], Tongxin Xie MD, PhD[3], Liang Yang PhD[1], Andrew Hefner BS[2], Meng Gao MBBS, PhD[3], Mitchell J. Frederick, PhD[4], Sahil Seth PhD[5], Mohamed Abdelhakiem MD[2], Beth M. Beadle MD, PhD[6], Faye Johnson MD, PhD[7], Jing Wang PhD[8], Li Shen MS[8], Timothy Heffernan PhD[5], Aakash Sheth BS[9], Robert Ferris MD, PhD[10], Jeffrey N. Myers MD, PhD[3], Curtis R. Pickering, PhD[3,*], Heath D. Skinner MD, PhD[2,*,#]

[1] *Department of Experimental Radiation Oncology, University of Texas, MD Anderson Cancer Center, Houston, USA.*

[2] *Department of Radiation Oncology, University of Pittsburgh, UPMC Hillman Cancer Center, Pittsburgh, USA.*

[3] *Department of Head and Neck Surgery, University of Texas, MD Anderson Cancer Center, Houston, USA.*

[4] *Department of Otolaryngology-Head & Neck Surgery, Baylor College of Medicine, Houston, USA.*

[5] *Institute for Applied Cancer Science, University of Texas, MD Anderson Cancer Center, Houston, USA.*

[6] *Department of Radiation Oncology, Stanford University, Stanford, California, USA*

[7] *Department of Thoracic and Head and Neck Medical Oncology, University of Texas, MD Anderson Cancer Center, Houston, USA.*

[8] *Department of Biostatistics, University of Texas, MD Anderson Cancer Center, Houston, USA.*

[9] *Robert Wood Johnson Medical School, Rutgers University, New Brunswick, USA.*

[10] *Department of Otolaryngology, University of Pittsburgh, UPMC Hillman Cancer Center, Pittsburgh, USA*

[*] contributed equally

 # Corresponding author:

Heath D. Skinner, MD, PhD

UPMC Hillman Cancer Center

5117 Centre Ave, Suite 2.6

Pittsburgh, PA, 15213-1862

Phone: (412) 623-3275

Email: skinnerh@upmc.edu

No conflicts of interest related to the manuscript are reported by any of the co-authors.

Summary

In this study we found that CREBBP/EP300 mutations drive clinical radioresistance, potentially due to a gain of function leading to hyperacetylation. Inhibition of histone acetyltransferase activity combined with radiation in tumors harboring these mutations, leads to synthetic cytotoxicity, via inhibition of homologous recombination.

Abstract

Head and neck cancer (HNSCC) harbors few directly targetable mutations; however, several may be sensitive to synthetic cytotoxicity. In this manuscript we examine whole exome sequencing in human HNSCC tumors, with mutations in CREBBP and EP300 or CASP8 associated with poor outcome. We then performed in vivo shRNA screening to identify targets associated with synthetic cytotoxicity in tumors harboring these mutations. This identified CREBBP/EP300 as a target for synthetic cytotoxicity in combination with radiation in cognate mutant tumors. Further in vitro and in vivo studies confirmed this phenomenon was due to repression of homologous recombination following DNA damage and can be reproduced using chemical inhibition of histone acetyltransferase (HAT), but not bromodomain function. Additionally, at least some mutations in CREBBP lead to a broadly hyperacetylated state, representing a previously undescribed gain of function phenotype that drives radioresistance and is sensitive to HAT inhibition. These findings represent a both a novel mechanism of treatment resistance and an avenue for genomically-driven treatment.

Background

Survival outcomes for head and neck squamous cell carcinoma (HNSCC) have remained largely unchanged for the past two decades. The treatment backbone for this malignancy remains ionizing radiation, either alone or in combination with surgical resection and/or cytotoxic chemotherapy. At present, there is a paucity of viable biologically driven radiosensitizers and only one clinically utilized biomarker in this malignancy, the presence of the human papillomavirus (HPV). In patients with HPV-negative cancers, several prognostic markers have been investigated (Skinner et al., 2012; Hess et al., 2019; Theodoraki et al., 2018; Liu et al., 2018; Kang et al., 2015); however, validation of these markers is limited, and clinical integration largely nonexistent.

Tumor genomic alterations can lead to increased susceptibility to a targeted therapy (synthetic lethality or synthetic cytotoxicity). The most common example of this phenomenon remains increased sensitivity of BRCA1 altered tumors to PARP inhibition (Fong et al., 2009). However, most large-scale screening approaches using cell lines with known genomic status have not exposed the cells to radiation and, thus, have not identified tumor mutations or alterations that can sensitize to radiation treatment (Huang et al., 2020). Genomically-driven radiosensitizers have the potential of only affecting the mutated cancer cells, and not normal cells, which would provide a clinically meaningful improvement over current radiosensitizers.

Additionally, most anti-neoplastic agents tested in the pre-clinical setting ultimately fail to be translated to the clinic due to multiple factors, including the artificial nature of *in vitro* systems and unforeseen toxicity (Gillet et al., 2013; Katt et al., 2016).

Targets identified as radiosensitizers in an *in vitro* model, may underperform *in vivo* due to complex interactions within the tumor itself. Additionally, the same microenvironment interactions could be potential targets for radiosensitization and may not be readily identified using *in vitro* screening techniques.

In the current investigation, we analyzed tumor tissues from patients with HNSCC treated with radiation therapy, identifying mutations associated with poor outcomes following radiation, and subsequently analyzed *in vivo* screening data to identify potential targets for synthetic cytotoxicity in tumors harboring these mutations. These data led to the identification of histone acetylation as a novel target in HNSCC, potentially driven by due to a gain of function in certain classes of CREBBP mutants, with less function inhibitory domain, leading to a basal hyper acetylated state and a dependency on homologous recombination for DNA damage repair. This is a novel approach that exploits the genetic modifications in these tumors, and their potential impact on radiation sensitivity, to identify a potential therapeutic strategy to overcome radiation resistance in a targeted fashion.

Results

Mutations in CASP8 or the CBP-p300 coactivator family (CREBBP and EP300) are associated with outcome following radiation in HNSCC.

We identified a cohort of patients within the Head and Neck Cancer Genome Atlas (TCGA) that were treated with surgery and adjuvant radiation therapy (Supplemental Table 1) and queried for genes mutated at ≥10% frequency (high enough for potential clinical utility) to determine their relationship to overall survival (Fig. 1A). The genes CREBBP and EP300 were combined into a single category (CBP-p300

coactivator family) because of their high genetic and functional similarity. Only 3 genes (TP53 (p=0.015), CASP8 (p=0.055) and CREBBP/EP300 (p=0.046) were associated with OS, as was the presence of HPV (p=0.002) (47 patients, 17.4%) (Figure 1A). Tumor stage (p=0.69), nodal stage (p=0.61), and tumor site (p=0.79) were not significantly associated with survival in this population; this is likely due to the similar clinical characteristics of the selected cohort, all of whom had advanced stage disease treated with combined modality therapy. While TP53 was associated with OS in patients who did not receive radiation (HR 1.52, p=0.053), CASP8 (p=0.41) and CREBBP/EP300 (p=0.89) were not, indicating that in the latter genes this phenomenon may be dependent upon radiation response.

Because the TCGA includes a cohort of patients with heterogeneous treatments and without details of patterns of failure (particularly the difference between LRR and DM), we examined patient outcomes in a more uniformly treated cohort of patients within this group, in which treatment and patterns of failure details were enumerated (Fig. 1 B-E). This subset included 94 patients with HPV-negative HNSCC treated uniformly with surgery and post-operative radiation (Clinical characteristics in Supplemental Table 1). In this analysis, TP53 (as a binary variable), was not associated with OS or LRR (Fig. 1B & C). Mutations in both CASP8 and the CBP-p300 coactivator family were associated with significantly reduced overall survival and higher rates of LRR in this patient population (Fig. 1B-E).

The presence of CDKN2A mutation was associated with decreased time to distant metastasis (DM), but it did not achieve statistical significance (p=0.08). No other mutation examined was associated with time to distant metastasis (DM).

CREBBP, EP300 or dual specificity protein kinase (TTK) inhibition in combination with radiation in CREBBP/EP300 mutated tumors leads to synthetic cytotoxicity.

Because of the observed poor outcomes in tumors with mutations in either CASP8 or CREBBP/EP300, we explored avenues for synthetic cytotoxicity associated with either. To accomplish this, we performed *in vivo* shRNA library screens in tumors generated from 5 HNSCC cell lines of varying genetic background and HPV status (HPV-positive: UM-SCC-47 & UPCI-SCC-152), HPV-negative: UM-SCC-22a, HN31 & Cal 27) treated with radiation (Supplemental Table 3). Two libraries were used: one encompassing most genes known to be targeted by available anti-neoplastic agents currently in clinical use or in clinical trials and the second targeting the DNA-damage repair pathway (Supplemental Table 4).

To determine a gene level summary estimate of the impact of knock-out of each gene, we performed redundant shRNA analysis (RSA) to generate log p-values for each gene for both irradiated and unirradiated tumor (Figure 2A). In the current study, the focus is primarily on the synthetic cytotoxicity in combination with radiation, thus targets preferentially associated with increased response to radiation (below and to the right of the blue dashed line in Fig. 2A) were selected for further study. The RSA log p-values and fold change for each of these targets were compared between either CASP8 wild type and mutant tumors (UM-SCC-47, UM-SCC-22a & CAL27 vs. HN31 & UPCI-SCC-152) (Fig. 2B) or CREBBP/EP300 wild type and mutant tumors (HN31 & CAL27 vs. UM-SCC-47, UPCI-SCC-152 & UM-SCC-22a) (Fig. 2C). While no differences were observed in the comparison of CASP8 wild type and mutant tumors in either of the libraries, several targets seemed to preferentially increase sensitivity to radiation in

CREBBP/EP300 mutant tumors (Fig. 2C-E). Specifically, inhibition of the CREBBP and EP300 genes themselves as well as the dual specificity protein kinase (TTK) were associated with increased *in vivo* sensitivity to radiation in the CREBBP/EP300 mutant but not wild type tumors in the screen.

Inhibition of CREBBP or EP300 expression leads to in vitro radiosensitization, but only in the presence of CBP-p300 coactivator family mutants.

To validate the genomic association between the CREBBP/EP300 mutation and synthetic cytotoxicity with CREBBP or EP300 shRNA and radiation, we performed targeted knockdown (KD) across an expanded set of cell lines. We utilized shRNA KD to either CREBBP or EP300 in six HNSCC cell lines (Fig. 3 and Supplemental Fig. 1) of varying CREBBP/EP300 mutation status (see Supplemental Table 3 for details). These cell lines were then treated with radiation, and clonogenic survival was assayed as described in the Supplemental methods (Fig. 2F). Similar to our *in vivo* screening results, CREBBP or EP300 KD was associated with increased sensitivity to radiation. However, the sensitivity appeared only in the context of a mutation in the cognate gene. For example, CREBBP KD, but not EP300, led to significant radiosensitization in the CREBBP mutant cell line UM-SCC-22a, which is EP300 wild type. Similarly, EP300 KD, but not CREBBP, led to significant radiosensitization in the EP300 mutant cell line UMSCC25 that is wild type for CREBBP. This pattern was consistently observed over all cell lines tested (Fig. 2F).

CREBBP inhibition leads to increased apoptosis and decreased BRCA1 foci formation following radiation in mutant cells.

To further evaluate the observed radiosensitization, we examined apoptosis in multiple cell lines expressing shRNA to CREBBP (Fig. 3A & B). The combination of CREBBP inhibition and radiation led to dramatically increased TUNEL staining in CREBBP mutant (but not wild type) cell lines (Fig. 3A). Similar results were observed on immunoblot examining caspase-3 cleavage via immunoblot as described in the Supplemental methods (Fig. 3B). We also examined the DNA damage response via immunofluorescence staining of DNA damage foci (Fig. 3C). Interestingly, the induction of ɣ-H2AX was greater in CREBBP inhibited cell lines that harbored CREBBP mutations, but not those harboring wild type CREBBP (Fig. 3C). Conversely, BRCA1 foci induction was significantly reduced following radiation in CREBBP inhibited cell lines in all the CREBBP mutant cell lines and HN30, which is both p53 and CREBBP wild type (Fig. 3C). However, ɣ-H2AX induction was also less in HN30 following radiation in CREBBP KD. Irrespective of mutational status, inhibition of CREBBP generally had little effect on 53BP1 foci formation following radiation (Fig. 3C).

Knockdown of CREBBP leads to dramatic in vivo radiosensitization.

We further evaluated the therapeutic potential of targeting CREBBP using two separate *in vivo* models of HNSCC. In the first study, we used the CREBBP mutant cell line UM-SCC-47 to generate tumors in the mouse flank. Tumors were treated with 2 Gy x 8 days, in a fractionation scheme designed to recapitulate that used in patients, albeit to a much lower dose (16 Gy total vs. 70 Gy in the clinic). In this experiment, radiation or CREBBP KD (using two distinct shRNA constructs) alone had minimal to modest effect; however, the combination led to a profound tumor growth delay and improved survival (Fig. 4A & B). Indeed, at the conclusion of the tumor growth delay experiment, 5

tumors in the irradiated shCREBBP-2 group (45%) and 7 tumors in the irradiated shCREBBP-3 group (64%) had regressed below the limits of detection. An additional separate experiment was performed to determine apoptosis, with TUNEL staining dramatically increased in the combined shCREBBP and radiation groups 8h following the final dose of radiation (2 Gy x 8 d) compared to both the irradiated shControl tumors and unirradiated CREBBP knock down tumors (Fig. 4C). In an independent CREBBP mutant, we performed a similar experiment using tumors derived from UMSCCC 22a cells (Fig. 4D). While inhibition of CREBBP alone had a significant effect in this model, we again observed a profound radiosensitization compared to the irradiated control tumors. In this model, virtually all the irradiated tumors in both CREBBP knockdown groups regressed below the limits of detection.

Inhibition of CBP and p300 histone acetyltransferase (HAT), but not bromodomain function, leads to synthetic cytotoxicity associated with repression of HR.

To further examine the therapeutic relevance of the observed synthetic cytotoxicity in HNSCC, we utilized several chemical inhibitors of CREBBP and/or EP300 function: 1) ICG-001, a CBP specific inhibitor that is thought to inhibit the interaction between CBP and β-catenin, although it is also known to have β-catenin independent effects (note: PRI-724 is an active enantiomer of ICG-001); 2) GNE-272, a bromodomain specific inhibitor for both CREBBP and EP300; 3) A-485, a histone acetyltransferase inhibitor specific for CREBBP and EP300 (note: A-486 is an inactive analog and used as a negative control). Similar to shRNA-based inhibition of CREBBP, ICG-001 led to significant *in vitro* radiosensitization on clonogenic assay, but only in those cell lines harboring a CREBBP mutation (Fig. 5A-D). This effect was largely due

to increased apoptosis following the addition of ICG-001 to radiation (Fig. 5E). Although the enantiomer of ICG-001, PRI-724, is actively in clinical trial development, neither of these agents target p300, and as predicted, we did not observe synthetic cytotoxicity in a wild type or an EP300 mutant cell line (Fig. 5C & D). Thus, to maximize the clinical impact of the observed synthetic cytotoxicity, we utilized additional inhibitors, currently in clinical development, that inhibit both CBP and p300 function. We initially tested GNE-272, a bromodomain inhibitor; however, this agent had no effects on sensitivity to radiation on clonogenic assay (Supplemental Fig. 2), independent of CREBBP or EP300 status. However, the HAT inhibitor A-485, but not the inactive A-486 analog, led to a profound radiosensitization in cell lines harboring a mutation in either CREBBP or EP300 (Fig. 6A), but not in wild type cell lines (Fig. 6B). The observed radiosensitization was largely due to increased apoptosis following the combination of A-485 and radiation (Fig. 6 C & D).

Because of the observed effects of shCREBBP on BRCA1 foci formation following radiation, we wished to evaluate the relationship between HAT inhibition and homologous recombination directly via iScel assay (Liu et al., 2018). Due to the inability to reliably express the required plasmids in HN cells, we utilized additional lung cancer lines which also harbor mutations in either CREBBP or EP300 (Fig. 6 E & F). Treatment with A485 led to repression of HR in CREBBP or EP300 mutant cell lines, but not in wild type (Fig. 6E) and had similar effects on clonogenic survival (Fig. 6F), with decreased survival in both mutant lines following exposure to A485 and radiation, but not in the wildtype line.

Histone acetylation is associated with synthetic cytotoxicity following CBP/p300 targeting in HNSCC.

Due to the observed synthetic cytotoxicity following HAT inhibition, we further investigated histone acetylation status in HNSCC cell lines following combination treatment. As expected, treatment with A-485 inhibited histone acetylation at H3K18 and H3K27 in HN5 and UM-SCC-22a cells (Fig. 7A). Both cell lines harbor mutations in either CREBBP and/or EP300 and exhibit synthetic cytotoxicity when HAT inhibition is combined with radiation. Interestingly, FaDu, a CREBBP/EP300 wild type cell line with no observed synthetic cytotoxicity, showed no effect on histone acetylation following treatment with HAT inhibitor at baseline or following radiation treatment. Similar effects on histone acetylation were observed following the expression of shRNA specific to CREBBP (Fig. 7B) and treatment with ICG-001 (Fig. 7C).

The observed synthetic cytotoxicity is not CREBBP or EP300 expression level dependent.

One potential explanation for the observed synthetic cytotoxicity is a simple dose-dependency. Namely, if basal levels of CREBBP or EP300 are significantly diminished in mutant cells (and tumors), a more profound inhibition is possible, leading to a more pronounced phenotype. Thus, the observed effect may be due to a more complete inhibition of the protein in the setting of a loss of function mutation. To further explore this hypothesis, we examined basal expression in HNSCC cell lines and tumors in the context of various CREBBP and EP300 mutations. Interestingly, basal CREBBP and EP300 gene expression in the cell lines used in this study were not directly associated with underlying mutation (Supplemental Fig. 3A). Moreover, in a panel of 82

HNSCC cell lines, neither CREBBP nor EP300 mutation was directly associated with mRNA expression (Supplemental Fig. 3B). Similarly, neither CBP nor p300 proteins were associated with mutation in the cell lines used in this study (Supplemental Fig. 3C).

In clinical samples from the TCGA HNSCC cohort, no significant difference in CREBBP or EP300 gene expression was observed in mutant tumors (Supplemental Fig. 3D). Moreover, even in the context of nearly complete inhibition of CREBBP protein expression (Fig. 3B & Supplemental Fig. 1) neither HN31 nor HN30 (CREBBP wild type cell lines) were sensitized to radiation (Fig. 2F). Conversely, incomplete inhibition of EP300 (in the case of EP300 mutants HN5 and HN30) led to significant radiosensitization (Fig. 2F & Supplemental Fig. 1).

Selected mutations in CREBBP exhibit increased acetylation activity consistent with gain of function and potentially mediating response to radiation.

Previously, mutations within the inhibitory TAZ domain of CBP have been linked to increased histone acetylation (Ghandi et al., 2019). Because of this observation, we evaluated two of our cell lines (UM-SCC-22a and UM-SCC-17b) with similar mutations (Fig. 8 A & B). Compared to wild type cells, these cell lines exhibited profoundly higher levels of acetylation of several histone marks as well as increased global protein acetylation (Fig. 8A). Additionally, CBP protein itself was acetylated at dramatically higher levels compared to wild type cells. As expected, the HAT inhibitor A485 dramatically inhibited the observed acetylation in both mutant cell lines (Fig. 8B).

We then forced CREBBP wild type (293T and HN31) cells to express full length or a representative inhibitory region mutant (Q1773X). In both lines, expression of the

mutant led to a profound increase in CBP auto-acetylation and global protein lysine-acetylation that was not observed following forced expression of wild type CBP (Fig. 8C). Similarly, forced expression of mutant CBP led to increased acetylation at H3K18 and H3K27 histone marks (Fig. 8 D). Additionally, we specifically examined the effects of mutant CBP on BRCA1 acetylation, which was similarly increased following forced expression of mutant CBP compared to wild type (Fig. 8 E). We then examined the potential effects of this acetylation due to CREBBP mutation on response to radiation. As expected, neither CRISPR KO nor forced expression of WT CBP in wild type HN31 cells had any effect on clonogenic survival following radiation (Fig. 8F). Interestingly, in UM-SCC-22a expressing only mutant CBP, cells became more resistant to radiation, an effect that was reversed by forced expression of WT CBP (Fig. 8E).

Discussion

The treatment of HNSCC has largely remained unchanged for decades, with little (or no) integration of biologically relevant information to understand prognosis or to motivate treatment paradigms. In this study, two cohorts of HNSCC tumors were studied (TCGA and institutional data) with identification of promising mutations associated with poor response that utilized to generate synthetic cytotoxicity with radiation and potentially associated with a gain function for hyperacetylation.

Three unexpected genes emerged from this combined analysis, specifically CASP8 and the CBP-p300 coactivator family (CREBBP and EP300), mutations in all of which were associated with dramatically higher rates of treatment failure. This may not be surprising in the case of CASP8, as this gene is intimately involved in apoptosis and one might conclude that a simple blocking of apoptosis is the sole explanation of this

phenomenon. However, the response of most solid epithelial tumors to conventional radiation is not classical apoptosis, but rather alternative modes of cell death, most prominently mitotic catastrophe (Eriksson and Stigbrand, 2010; Roninson et al., 2001). Thus, deficient apoptosis in this setting may be an insufficient explanation of this phenomenon and further study of the role of CASP8 in other modes of cell death is necessary (Uzunparmak et al., 2020).

Mutations in the related histone acetyltransferases, CREBBP and EP300, were also associated with treatment failure following radiation. The relationship between mutation in CREBBP or EP300, inhibition of CREBBP or EP300, and treatment with DNA damaging agents is understudied. CREBBP and EP300 are homologous multifunctional bromodomain-containing acetyltransferases that can regulate many proteins and pathways. They have significantly overlapping functions, and a large number of chemical inhibitors are being developed for clinical use targeting both with approximately equal efficacy. Taken together, CREBBP and EP300 are collectively mutated in 13% of HNSCC and 14% of all squamous cancers (Cancer Genome Atlas Network, 2015), with similar frequencies in both HPV-positive and HPV-negative disease. Missense mutations are clustered in the acetyltransferase domain, and there is a reasonable frequency of truncating mutations (~20%). We have observed a similar pattern of mutations in our panel of HNSCC cell lines. Additionally, many of these mutations are heterozygous, indicating possible haploinsufficiency, as has been seen for the chromatin modifying genes in the BAF complex (Kadoch and Crabtree, 2015). Although these genes are mutated in HNSCC, they have not been extensively studied

in this tumor type. Very little is known about their function as tumor suppressor genes or what impact they have on tumor progression or response to therapy.

Given the limitations in *in vitro* screening analyses, *in vivo* shRNA screening was analyzed in the context of either CASP8 or CREBBP/EP300 mutations, searching for synthetically cytotoxic combinations with radiation. Although we did not observe synthetically cytotoxic targets in CASP8 tumors, we identified several in the CREBBP/EP300 mutant tumors, including the CREBBP and EP300 genes themselves. Both *in vitro* and *in vivo*, we observed a similar phenomenon, namely that inhibition of either gene individually led to a dramatic sensitization to radiation, but only in the context of their cognate mutation. The effect was associated with both increased induction of DNA damage following radiation as well as inhibition of homologous recombination (HR), leading to increased early apoptosis. This latter effect is interesting in that most HNSCC cell lines and tumors are relatively resistant to apoptosis following DNA-damaging therapies, such as radiation or chemotherapy (Skinner et al., 2012; Roninson et al., 2001; Prokhorova et al., 2019; Osman et al., 2015; Gadhikar et al., 2013). Thus, this phenotype represents an unexpected but important shift in response.

To examine the potential for therapeutic intervention of these findings, we tested inhibitors of specific CREBBP or EP300 functions in combination with radiation. While bromodomain inhibitors exhibited no synthetic cytotoxicity, the use of a HAT inhibitor exhibited dramatic sensitization to radiation, but only in the context of a mutation in either CREBBP or EP300. This points towards the histone acetylase function of either protein to be critical for the observed phenomenon. Indeed, inhibition of key histone marks was observed only in mutant cells that exhibited synthetic cytotoxicity.

We have seen that the combination of HAT inhibition and DNA damage leads to a synthetic cytotoxicity in tumors harboring mutations in the CBP-p300 coactivator family. The mechanism of this phenomenon is likely complex. The most well-characterized functions for CBP and p300 are as protein acetyltransferases. The primary targets of this acetylation are histone tails (H3K18, H3K27, H4K5/8/12/16) where they function to open the chromatin structure and facilitate gene expression. The dysfunction of either of these proteins leads to a loss of histone acetylation, a process that can affect DNA damage repair. Firstly, inhibition of CBP and p300 can transcriptionally repress BRCA1 via a lack of histone acetylation of that gene's promoter region and binding E2F1 (Ogiwara and Kohno, 2012). In that study, genes associated with non-homologous end joining (NHEJ) were not associated with CBP/p300 modulation. We observed similar results in our own model, with the predominant effect appearing to be on HR. However, additional studies have linked CBP/p300 modulation of histone acetylation directly to both alterations of NHEJ or HR depending upon the study and cellular context (Ogiwara et al., 2011; Tamburini and Tyler, 2005; Qi et al., 2016). Thus, effects on DDR may be largely context dependent, varying with genetic background as well as with specific genetic insult.

As stated, the synthetic cytotoxicity observed in this study is dependent upon mutations in the CBP-p300 coactivator family. One previous study has identified an "addiction" to p300 in the context of CBP deletion, which was felt to replicate naturally occurring mutations in CREBBP (Ogiwara et al., 2016). However, we did not observe a synthetically lethal effect with p300 inhibition in CREBBP mutant cell lines in our model, either at baseline or in combination with radiation. We also did not observe the converse

in EP300 cell lines when CBP was inhibited. Thus, deletion of either protein may not recapitulate naturally occurring mutation in HNSCC.

Regarding the observed synthetic cytotoxicity, several explanations are possible. The simplest being that cell lines and tumors expressing mutations, particularly truncating mutations, in either gene potentially lead to less protein product. Thus, the phenomenon could be a simple dosing effect. However, we present several lines of evidence suggesting that this may be an incomplete explanation. Firstly, basal expression of either CREBBP or EP300 was not directly correlated with mutation in cell lines or clinical tumors. Moreover, the magnitude of inhibition of either CREBBP or EP300 did not predict response (i.e. complete inhibition of CBP in the context of a wild type cell line had no effect).

Indeed, the data support a potentially more complex hypothesis of a gain of function for at least some mutations in the CBP-p300 coactivator family. We observed high basal levels of both protein and histone acetylation in cell lines harboring mutations which truncate the protein after the HAT domain. Moreover, forced expression of similar mutations in wild type cell lines recapitulated this effect. Finally, unopposed expression of this mutant CBP led to increased resistance to radiation, which was reversed via either re-expression of wild type CBP or treatment with a HAT inhibitor. The concept of gain of function in this context is not wholly unprecedented; it has been shown previously that similar CREBBP/EP300 mutations are associated with increased histone acetylation at baseline in a large scale *in vitro* screen (Ghandi et al., 2019). If true, a basal hyper-acetylated state would have profound effects on DNA repair proteins such as BRCA1. Indeed, we demonstrated that BRCA1 was specifically acetylated by a

representative mutant form of CBP. As acetylation of BRCA1 is linked to an increase in its DNA-repair capability (Lahusen et al., 2018), this observation may speak to the importance of homologous recombination in the observed synthetic cytotoxicity phenotype. Moreover, increased acetylation of histones can lead to a relaxed chromatin state allowing for easier access of the DNA damage repair machinery and basal resistance to DNA-damage. Further studies will need to be performed to determine which specific mutations are required to exhibit this gain of function effect.

In conclusion, we have both identified novel prognostic markers of treatment failure in HNSCC as well as explored a novel synthetic cytotoxicity involving one of these biomarkers, mutated CREBBP/EP300. This synthetic cytotoxicity appears to specifically involve effects on DNA damage repair, leading to a HR deficiency following DNA damage and leading to increased apoptosis. Moreover, a potential gain of function effect in mutated cell lines may be driving this phenomenon leading to a basal hyper-acetylated state affecting BRCA1 function. Finally, the observed synthetic cytotoxicity can be induced in both CREBBP and EP300 mutated models using a HAT inhibitor, which is currently being explored for clinical trial use, and thus could be translated clinically to improve outcomes in this deadly disease.

Materials and Methods

Clinical data

This study was approved via appropriate Institutional Review Boards. The initial patient cohort consisted of the Head and Neck TCGA group that satisfied the following criteria: i) whole exome sequencing data is available and ii) were denoted in the TCGA records as having received radiation as part of their initial therapy (Clinical

characteristics in Supplemental Table 1). Of the 523 patients in the TCGA cohort, a total of 276 patients met these criteria. Whole exome sequencing from these tumors were examined for genes with mutations in ≥10% of tumors and significance on MutSig with the following genes meeting these criteria: TP53, FAT1, CDKN2A, NOTCH1, NSD1, CREBBP and EP300 (combined due to significant homology) and CASP8 (Campbell et al., 2018; Cancer Genome Atlas Network, 2015). A subset (n=94) of patients from this cohort have known specific treatment characteristics and patterns of failure analysis (Clinical characteristics in Supplemental Table 2). These patients were all treated with surgery and post-operative radiation with well-annotated outcomes, including loco-regional recurrence and distant metastasis. In addition to the above, all tumors in this subset cohort were HPV/p16-negative as demonstrated by immunohistochemistry (IHC) or in-situ hybridization (ISH). Overall survival was defined from time of diagnosis until death or last follow up. Time to loco-regional recurrence (LRR) or distant metastasis (DM) was defined as time from diagnosis until either an event or last follow up. Clinical variables examined included tumor stage, nodal stage, and primary tumor site. Univariate analysis was performed using Cox-regression (SPSS v25). Kaplan Meier curves were generated, and group comparisons were performed using log-rank statistics.

Cell Lines

HNSCC cell lines (UM-SCC-47, UM-SCC-22a, UM-SCC-25, UM-SCC-1, HN31, HN30, UM-SCC-17b, UPCI:SCC152, Cal-27, UD-SCC-2 and HN5) used in this study were generously supplied by Dr. Jeffrey Myers via The University of Texas MD Anderson Cancer Center Head and Neck cell line repository. HEK-293T, NCI-H520,

NCI-H2228, Calu-6, FaDu and Detroit562 were purchased form American Type Culture Collection (Manassas, VA). Cell lines were tested for mycoplasma and genotyped before experiments. See the Supplemental methods for more details.

TUNEL Assay

Following experimental treatments, all cells were collected including floating cells and TUNEL staining was performed using the APO-DIRECT Kit (BD Pharmingen) according to the manufacturer's protocol. Briefly, 1 million cells were fixed in 1% paraformaldehyde on ice for 30min. Cells were then washed in PBS and fixed in 70% ethanol overnight at -20C. Cells were washed twice with provided buffer then stained with 50ul of DNA labeling solution at 37C for 45min. Cells were then rinsed twice with provided buffer and resuspended in 300ul of rinse buffer. Cells were then analyzed by flow cytometry using the BD Accuri C6 flow cytometer (BD Biosciences) with 488nm laser, 533/30 filter and FL1 detector. 10,000 events were measured per sample.

Histone Extraction

Histone proteins were extracted from treated or untreated cells using a histone extraction kit (Abcam) according to the manufacturer's protocol. Briefly, cells were harvested, and pellet was obtained by centrifugation at 10,000 rpm for 5 minutes at 4˚C. The cells were re-suspended in 1X pre-lysis buffer and incubated at 4˚C for 10 minutes on a rotator and then centrifuged for one minute at 10,000 rpm at 4˚C. The cell pellet was re-suspended in lysis buffer at a concentration of 200 uL/10^7 cells and incubated on ice for 30 minutes, then centrifuged at 12,000 rpm for 5 minutes at 4˚C. The supernatant was collected and 300uL balance buffer-DTT was added per 1mL supernatant. The

quantity of protein extracted was measured with a DC protein assay kit (Bio-Rad, Hercules, CA, USA). 2-4 µg of protein were separated by western blot analysis as described previously.

Immunofluorescence Staining

Immunofluorescence was performed to measure quantitative differences in DNA damage repair and response. Cells were cultivated on cover slips placed in 35-mm cell culture dishes. At specified time points after exposure to radiation (2Gy), cells were fixed in 4% paraformaldehyde for 10 min at room temperature on shaker, briefly washed in phosphate-buffered saline or PBS (Biorad), and placed in 70% ethanol at 4°C overnight. These fixed cells were washed with PBS twice to remove ethanol and permeabilized with 0.1% IGEPAL (octylphenoxypolyethoxyethanol) for 20 min at room temperature on shaker, followed by blocking in 2% bovine serum albumin (Sigma) for 60 min, and then incubated with anti-γH2AX (1:400, Trevigen), 53BP1 (1:200, CST) or anti-BRCA1 primary antibody (1:500, Santa Cruz) overnight at 4°C. Next day fixed cells were washed three times with PBS and incubated for 45 minutes in the dark in secondary anti-mouse antibody conjugated to FITC to visualize γH2AX or BRCA1. Secondary anti-rabbit antibody conjugated to Cy3 was used to visualize 53BP1. DNA was stained with 4', 6-diamidino-2-phenylindole (Sigma) at 1:1000 (1 microgram/ml). Immunoreactions were visualized with an Olympus or Leica Microsystems microscope (Wetzlar, Germany), and foci were counted with Image J software (https://imagej.nih.gov/ij/).

Plasmids and shRNA Transfection

Packaging cell line HEK-293T was co-transfected with 3 microgram GIPZ lentiviral shRNAs specific for the CREBBP, EP300 gene or control(GE Dharmacon) and lentiviral vectors DR8.2 and VSVG (Addgene) . Two and three days after transfection , virus containing media was filtered through a 0.45 micron PVDF syringe filter and polybrene was added (1:2000). Target cells were transduced with virus for 4-6h and were subjected to puromycin antibiotic selection. Pooled knockdown cells and counterparts shControl cells were assessed for CREBBP protein expression by immunoblotting. shRNA sequences are given as follow:

shRNA CREBBP	2# TRCN0000006486	GCTATCAGAATAGGTATCATT
	3# TRCN0000006487	GCGTTTACATAAACAAGGCAT
shRNA EP300	#2 TRCN0000039884	5`-CCAGCCTCAAACTACAATAAA-3`
	#4 TRCN0000039886	5`-CCCGGTGAACTCTCCTATAAT-3`
	#5 TRCN0000039887	5`-CGAGTCTTCTTTCTGACTCAA-3`

Site-directed mutagenesis

Site-directed mutagenesis was performed using 50ng of KAT3A / CBP (CREBBP) (NM_004380) Human Tagged ORF Clone (OriGene) as the dsDNA template. This was carried out using the QuickChange II XL Site-Directed Mutagenesis Kit (Agilent Technologies) according to the manufacturer's protocol with the following exception: One Shot™ Stbl3™ Chemically Competent E. coli (Invitrogen) was used for transformation rather than the XL10-Gold Ultracompetent Cells supplied with the kit because of the dependency on chloramphenicol selection already found in the full length CREBBP vector. Mutagenic oligonucleotide primers were designed using Agilent

QuickChange Primer Design program and purchased from Sigma-Aldrich with PAGE purification with the following sequences:

5'-tggatgcagcgctagatgctcagccgg-3'

5'-ccggctgagcatctagcgctgcatcca-3'

Following transformation, single colonies were selected on LB plates containing 34ug/mL Chloramphenicol, expanded in LB broth containing 34ug/mL Chloramphenicol overnight, and extracted with a QIAfilter midi kit (Qiagen).Sanger sequencing was utilized to confirm the presence of the desired mutation. Mutant plasmids were directly transfected into cell lines using GeneJet transfection reagent (SignaGen Labs) or packaged in 293T for lentiviral infection.

HR specific DRGFP/DNA repair assay

Calu6 and H520 cells were transfected with 3ug DRGFP substrate using PEI. H2228 cells were electroporated with 3ug DRGFP substrate using reagent T (Amaxa Cell Line Nucleofector Kit T, Lonza), program X-001 on the Nucleofector 2b (Lonza). Puromycin selection was performed with 2ug/ml for Calu6 and H2228 or 4ug/ml for H520. DRGFP expressing cells were electroporated in reagent T for H520 and H2228 or reagent L (Amaxa Cell Line Nucleofector Kit L, Lonza) for Calu6 with 10ug I-SceI using program X-005 for Calu6, T-020 for H520 or X-001 for H2228. Following electroporation, cells were washed with media and transferred into 6 well dishes with 2ml media/well containing either DMSO, 3uM A485 or 3uM A486 and incubated for 48h. Cells were then trypsinized, washed with PBS and resuspended in 300ul of PBS containing 1% FBS, and flow cytometry was run to detect GFP using the BD Accuri C6 flow cytometer (BD Biosciences).

Mouse xenograft model

In vivo studies were performed following Institutional Care and Use Committee (IACUC) approval. Male athymic nude mice (6-8 weeks old, ENVIGO/HARLAN, USA) were randomly assigned to one of 6 treatment groups of 15 mice each for each cell line tested. Tumor cells (2×10^6 in 0.1 mL of serum-free medium) were injected subcutaneously in the right dorsal flank of each mouse. After palpable tumors had developed, tumor diameters were measured with digital calipers, and tumor volume was calculated as A × B2 × 0.5, where A represents the largest diameter and B the smallest diameter. When the tumor volumes reached approximately ~150 mm^3, tumors were irradiated with 16 Gy (2 Gy/day x 8 days) and tracked for approximately 4 weeks for tumor growth delay experiments (n=~10/group). At that time, the experiment was completed and tumors harvested. For in vivo TUNEL assay, tumors were collected 8 h after the last radiation treatment (n=5/group). A tumor growth delay experiment was performed in a similar fashion using UM-SCC-22A shControl, UM-SCC-22A shCREBBP#2, and UM-SCC-22A shCREBBP#3. To compare tumor growth delay between groups, linear regression of the growth curve was calculated for each group and the slope of each curve was compared between groups using Graph Pad Prism (v8.0).

***In vivo* TUNEL assay**

Paraffin embedded sections (4μm) of UMSCC47 tumor xenografts were mounted on coated slides and sent to HistoWiz Inc. (histowiz.com) for TUNEL staining and quantification. TUNEL staining was performed using a Standard Operating Procedure and fully automated workflow with Deadend colorimetric TUNEL system from Promega.

After staining, sections were dehydrated and film coverslipped using a TissueTek-Prisma and Coverslipper (Sakura). Whole slide scanning (40x) was performed on an Aperio AT2 (Leica Biosystems). Images were analyzed using Halo (version 2.3.2089.34) image analysis software from Indica Labs (Albuquerque, NM). Regions of interest were selected. TUNEL staining was segmented using the CytoNuclear algorithm. Total cell counts were thresholded into low, medium, and high intensity staining bins.

In vivo shRNA screening

A loss-of-function screen using two pooled shRNA libraries (targets in Supplemental Table 4), generally, using the method described Carugo et al., with the addition of fractionated radiation (Carugo et al., 2016). These libraries targeted genes associated with DNA damage repair (derived from Gene Ontology) or genes known to be “druggable”.

Each library was cloned into the pRSI17 vector (Cellecta) and packed into lentivirus particles. HNSCC cell lines were infected *in vitro* through spinfection with virus containing the library at a low MOI (~20% infected cells as measured by flow cytometry) in order to minimize superinfection of cells. Cells were selected with puromycin for at least 2 days and grown *in vitro* for <3 population doublings prior to injection of 4 million cells subcutaneously in nude mouse flank. An additional 2 million cells from the day of injection were collected as a frozen reference cell pellet.

Pilot studies were performed to: i) examine the frequency of tumor initiating cells (TIC) and determine whether the cell line could maintain shRNA library complexity *in vivo* and

ii) identify the dose of radiation needed to achieve ~20% tumor reduction for each model by the conclusion of the experiment.

For the screening experiment itself, xenografts were treated with 2 Gy/day of radiation once the tumor had reached approximately 100 mm^3 to a total dose of 6-10 Gy depending upon the model. Following treatment, the tumors were allowed to grow for approximately 2 weeks (volume ~ 500mm3). DNA was isolated from tumor and reference cells, amplified, and sequenced on Illumina sequencers as previously described (Carugo et al., 2016).

Hairpin counts were normalized to counts per million (CPM) per sample to enable comparison across samples. For each sample, (log2) fold-change of each hairpin in the tumor was calculated compared to the level in the reference pellet. A hairpin summary measure per cell line was derived from the median of quantile transformed log2 FC across replicates. Next, a modified version of the redundant siRNA activity (RSA) algorithm (Birmingham et al., 2009) was used to derive a gene level summary measure per cell line. RSA attempts to provide a gene level summary estimate of the impact of knock-out of the gene by calculating a stepwise hypergeometric test for each hairpin in a gene. Similar to GSEA, it is based on evidence from multiple hairpins of a gene showing an impact of cellular fitness. Our modifications were to ensure both that at least 2 hairpins were used when calculating the minimum p-value (in RSA) and that hairpins ranking above luciferase controls were not used when determining the minimum p-value. Quantile rank of luciferase controls barcodes was determined through evaluation across all experiments; on an average luciferase barcodes ranked >0.6 on the quantile

transformed log2fc scale, so hairpins with quantile transformed log2fc > 0.6 were not used for the gene-level RSA score.

Contributions

HS and CP directed the experiments and analyzed the clinical data. MF assisted in the planning, direction and analysis of the in vivo screening experiments. MK, TX, LY, TH and SS directly performed the *in vivo* screening and/or processed and analyzed the resultant samples. MK, KB and DM generated the stable KD cell lines. DM, JM, KB, MG, AS, AH and MK performed the in vitro experiments (clonogenic survival, immunoblot, histone extraction, DNA foci, TUNEL assay). FJ, JW and LS generated and/or analyzed the HNSCC cell line RNA Seq and mutation data. BB, JM and RF reviewed and evaluated the clinical data analysis. MK initiated this study, which was then continued by DM. This determined co-first author order.

Funding

This work was supported by: i) the National Cancer Institute R01CA168485-08 (HS) and P50CA097190-15 (RF), ii) the National Institute for Dental and Craniofacial Research R01 DE028105 (HS) and R01DE028061 (HS and CP), and iii) The Cancer Prevention Institute of Texas RP150293 (HS and CP).

References

Birmingham, A., L.M. Selfors, T. Forster, D. Wrobel, C.J. Kennedy, E. Shanks, J. Santoyo-Lopez, D.J. Dunican, A. Long, D. Kelleher, Q. Smith, R.L. Beijersbergen, P. Ghazal, and C.E. Shamu. 2009. Statistical Methods for Analysis of High-Throughput RNA Interference Screens. *Nat. Methods*. 6:569–575. doi:10.1038/nmeth.1351.

Campbell, J.D., C. Yau, R. Bowlby, Y. Liu, K. Brennan, H. Fan, A.M. Taylor, C. Wang, V. Walter, R. Akbani, L.A. Byers, C.J. Creighton, C. Coarfa, J. Shih, A.D. Cherniack, O. Gevaert, M. Prunello, H. Shen, P. Anur, J. Chen, H. Cheng, D.N. Hayes, S. Bullman, C.S. Pedamallu, A.I. Ojesina, S. Sadeghi, K.L. Mungall, A.G. Robertson, C. Benz, A. Schultz, R.S. Kanchi, C.M. Gay, A. Hegde, L. Diao, J. Wang, W. Ma, P. Sumazin, H.-S. Chiu, T.-W. Chen, P. Gunaratne, L. Donehower, J.S. Rader, R. Zuna, H. Al-Ahmadie, A.J. Lazar, E.R. Flores, K.Y. Tsai, J.H. Zhou, A.K. Rustgi, E. Drill, R. Shen, C.K. Wong, Cancer Genome Atlas Research Network, J.M. Stuart, P.W. Laird, K.A. Hoadley, J.N. Weinstein, M. Peto, C.R. Pickering, Z. Chen, and C. Van Waes. 2018. Genomic, Pathway Network, and Immunologic Features Distinguishing Squamous Carcinomas. *Cell Rep.* 23:194-212.e6. doi:10.1016/j.celrep.2018.03.063.

Cancer Genome Atlas Network. 2015. Comprehensive genomic characterization of head and neck squamous cell carcinomas. *Nature*. 517:576–582. doi:10.1038/nature14129.

Carugo, A., G. Genovese, S. Seth, L. Nezi, J.L. Rose, D. Bossi, A. Cicalese, P.K. Shah, A. Viale, P.F. Pettazzoni, K.C. Akdemir, C.A. Bristow, F.S. Robinson, J. Tepper, N. Sanchez, S. Gupta, M.R. Estecio, V. Giuliani, G.I. Dellino, L. Riva, W. Yao, M.E. Di Francesco, T. Green, C. D'Alesio, D. Corti, Y. Kang, P. Jones, H. Wang, J.B. Fleming, A. Maitra, P.G. Pelicci, L. Chin, R.A. DePinho, L. Lanfrancone, T.P. Heffernan, and G.F. Draetta. 2016. In Vivo Functional Platform Targeting Patient-Derived Xenografts Identifies WDR5-Myc Association as a Critical Determinant of Pancreatic Cancer. *Cell Rep.* 16:133–147. doi:10.1016/j.celrep.2016.05.063.

Eriksson, D., and T. Stigbrand. 2010. Radiation-induced cell death mechanisms. *Tumour Biol. J. Int. Soc. Oncodevelopmental Biol. Med.* 31:363–372. doi:10.1007/s13277-010-0042-8.

Fong, P.C., D.S. Boss, T.A. Yap, A. Tutt, P. Wu, M. Mergui-Roelvink, P. Mortimer, H. Swaisland, A. Lau, M.J. O'Connor, A. Ashworth, J. Carmichael, S.B. Kaye, J.H.M. Schellens, and J.S. de Bono. 2009. Inhibition of poly(ADP-ribose) polymerase in tumors from BRCA mutation carriers. *N. Engl. J. Med.* 361:123–134. doi:10.1056/NEJMoa0900212.

Gadhikar, M.A., M.R. Sciuto, M.V.O. Alves, C.R. Pickering, A.A. Osman, D.M. Neskey, M. Zhao, A.L. Fitzgerald, J.N. Myers, and M.J. Frederick. 2013. Chk1/2 inhibition

overcomes the cisplatin resistance of head and neck cancer cells secondary to the loss of functional p53. *Mol. Cancer Ther.* 12:1860–1873. doi:10.1158/1535-7163.MCT-13-0157.

Ghandi, M., F.W. Huang, J. Jané-Valbuena, G.V. Kryukov, C.C. Lo, E.R. McDonald, J. Barretina, E.T. Gelfand, C.M. Bielski, H. Li, K. Hu, A.Y. Andreev-Drakhlin, J. Kim, J.M. Hess, B.J. Haas, F. Aguet, B.A. Weir, M.V. Rothberg, B.R. Paolella, M.S. Lawrence, R. Akbani, Y. Lu, H.L. Tiv, P.C. Gokhale, A. de Weck, A.A. Mansour, C. Oh, J. Shih, K. Hadi, Y. Rosen, J. Bistline, K. Venkatesan, A. Reddy, D. Sonkin, M. Liu, J. Lehar, J.M. Korn, D.A. Porter, M.D. Jones, J. Golji, G. Caponigro, J.E. Taylor, C.M. Dunning, A.L. Creech, A.C. Warren, J.M. McFarland, M. Zamanighomi, A. Kauffmann, N. Stransky, M. Imielinski, Y.E. Maruvka, A.D. Cherniack, A. Tsherniak, F. Vazquez, J.D. Jaffe, A.A. Lane, D.M. Weinstock, C.M. Johannessen, M.P. Morrissey, F. Stegmeier, R. Schlegel, W.C. Hahn, G. Getz, G.B. Mills, J.S. Boehm, T.R. Golub, L.A. Garraway, and W.R. Sellers. 2019. Next-generation characterization of the Cancer Cell Line Encyclopedia. *Nature*. 569:503–508. doi:10.1038/s41586-019-1186-3.

Gillet, J.-P., S. Varma, and M.M. Gottesman. 2013. The Clinical Relevance of Cancer Cell Lines. *JNCI J. Natl. Cancer Inst.* 105:452–458. doi:10.1093/jnci/djt007.

Hess, J., K. Unger, C. Maihoefer, L. Schüttrumpf, L. Wintergerst, T. Heider, P. Weber, S. Marschner, H. Braselmann, D. Samaga, S. Kuger, U. Pflugradt, P. Baumeister, A. Walch, C. Woischke, T. Kirchner, M. Werner, K. Werner, M. Baumann, V. Budach, S.E. Combs, J. Debus, A.-L. Grosu, M. Krause, A. Linge, C. Rödel, M. Stuschke, D. Zips, H. Zitzelsberger, U. Ganswindt, M. Henke, and C. Belka. 2019. A Five-MicroRNA Signature Predicts Survival and Disease Control of Patients with Head and Neck Cancer Negative for HPV Infection. *Clin. Cancer Res.* 25:1505–1516. doi:10.1158/1078-0432.CCR-18-0776.

Huang, A., L.A. Garraway, A. Ashworth, and B. Weber. 2020. Synthetic lethality as an engine for cancer drug target discovery. *Nat. Rev. Drug Discov.* 19:23–38. doi:10.1038/s41573-019-0046-z.

Kadoch, C., and G.R. Crabtree. 2015. Mammalian SWI/SNF chromatin remodeling complexes and cancer: Mechanistic insights gained from human genomics. *Sci Adv*. 1:e1500447. doi:10.1126/sciadv.1500447.

Kang, H., A. Kiess, and C.H. Chung. 2015. Emerging biomarkers in head and neck cancer in the era of genomics. *Nat. Rev. Clin. Oncol.* 12:11–26. doi:10.1038/nrclinonc.2014.192.

Katt, M.E., A.L. Placone, A.D. Wong, Z.S. Xu, and P.C. Searson. 2016. In Vitro Tumor Models: Advantages, Disadvantages, Variables, and Selecting the Right Platform. *Front. Bioeng. Biotechnol.* 4. doi:10.3389/fbioe.2016.00012.

Lahusen, T.J., S.-J. Kim, K. Miao, Z. Huang, X. Xu, and C.-X. Deng. 2018. BRCA1 function in the intra-S checkpoint is activated by acetylation via a pCAF/SIRT1 axis. *Oncogene*. 37:2343–2350. doi:10.1038/s41388-018-0127-1.

Liu, X., M. Kumar, L. Yang, D.P. Molkentine, D. Valdecanas, S. Yu, R.E. Meyn, J.V. Heymach, and H.D. Skinner. 2018. BAP1 Is a Novel Target in HPV-Negative Head and Neck Cancer. *Clin. Cancer Res. Off. J. Am. Assoc. Cancer Res.* 24:600–607. doi:10.1158/1078-0432.CCR-17-1573.

Ogiwara, H., and T. Kohno. 2012. CBP and p300 Histone Acetyltransferases Contribute to Homologous Recombination by Transcriptionally Activating the BRCA1 and RAD51 Genes. *PLOS ONE*. 7:e52810. doi:10.1371/journal.pone.0052810.

Ogiwara, H., M. Sasaki, T. Mitachi, T. Oike, S. Higuchi, Y. Tominaga, and T. Kohno. 2016. Targeting p300 Addiction in CBP-Deficient Cancers Causes Synthetic Lethality by Apoptotic Cell Death due to Abrogation of MYC Expression. *Cancer Discov.* 6:430–445. doi:10.1158/2159-8290.CD-15-0754.

Ogiwara, H., A. Ui, A. Otsuka, H. Satoh, I. Yokomi, S. Nakajima, A. Yasui, J. Yokota, and T. Kohno. 2011. Histone acetylation by CBP and p300 at double-strand break sites facilitates SWI/SNF chromatin remodeling and the recruitment of non-homologous end joining factors. *Oncogene*. 30:2135–2146. doi:10.1038/onc.2010.592.

Osman, A.A., M.M. Monroe, M.V. Ortega Alves, A.A. Patel, P. Katsonis, A.L. Fitzgerald, D.M. Neskey, M.J. Frederick, S.H. Woo, C. Caulin, T.-K. Hsu, T.O. McDonald, M. Kimmel, R.E. Meyn, O. Lichtarge, and J.N. Myers. 2015. Wee-1 kinase inhibition overcomes cisplatin resistance associated with high-risk TP53 mutations in head and neck cancer through mitotic arrest followed by senescence. *Mol. Cancer Ther.* 14:608–619. doi:10.1158/1535-7163.MCT-14-0735-T.

Prokhorova, E.A., A.Y. Egorshina, B. Zhivotovsky, and G.S. Kopeina. 2019. The DNA-damage response and nuclear events as regulators of nonapoptotic forms of cell death. *Oncogene*. 1–16. doi:10.1038/s41388-019-0980-6.

Qi, W., H. Chen, T. Xiao, R. Wang, T. Li, L. Han, and X. Zeng. 2016. Acetyltransferase p300 collaborates with chromodomain helicase DNA-binding protein 4 (CHD4) to facilitate DNA double-strand break repair. *Mutagenesis*. 31:193–203. doi:10.1093/mutage/gev075.

Roninson, I.B., E.V. Broude, and B.D. Chang. 2001. If not apoptosis, then what? Treatment-induced senescence and mitotic catastrophe in tumor cells. *Drug Resist. Updat. Rev. Comment. Antimicrob. Anticancer Chemother.* 4:303–313. doi:10.1054/drup.2001.0213.

Skinner, H.D., V.C. Sandulache, T.J. Ow, R.E. Meyn, J.S. Yordy, B.M. Beadle, A.L. Fitzgerald, U. Giri, K.K. Ang, and J.N. Myers. 2012. TP53 disruptive mutations lead to head and neck cancer treatment failure through inhibition of radiation-

induced senescence. *Clin. Cancer Res. Off. J. Am. Assoc. Cancer Res.* 18:290–300. doi:10.1158/1078-0432.CCR-11-2260.

Tamburini, B.A., and J.K. Tyler. 2005. Localized Histone Acetylation and Deacetylation Triggered by the Homologous Recombination Pathway of Double-Strand DNA Repair. *Mol. Cell. Biol.* 25:4903–4913. doi:10.1128/MCB.25.12.4903-4913.2005.

Theodoraki, M.-N., S.S. Yerneni, T.K. Hoffmann, W.E. Gooding, and T.L. Whiteside. 2018. Clinical Significance of PD-L1+ Exosomes in Plasma of Head and Neck Cancer Patients. *Clin. Cancer Res. Off. J. Am. Assoc. Cancer Res.* 24:896–905. doi:10.1158/1078-0432.CCR-17-2664.

Uzunparmak, B., M. Gao, A. Lindemann, K. Erikson, L. Wang, E. Lin, S.J. Frank, F.O. Gleber-Netto, M. Zhao, H.D. Skinner, J. Newton, A.G. Sikora, J.N. Myers, and C.R. Pickering. 2020. Loss of Caspase-8 function in combination with SMAC mimetic treatment sensitizes Head and Neck Squamous Carcinoma to radiation through induction of necroptosis. *bioRxiv*. 2020.04.17.039040. doi:10.1101/2020.04.17.039040.

Figure Legend

Figure 1. Whole exome sequencing identifies CASP8 and CREBBP/EP300 mutation significantly associated with treatment failure in HNSCC. A) Forrest plot of hazard ratios (HR) for Overall survival (OS) for TCGA patients known to have received radiation therapy. B & C) Forrest plot of HR for OS (B) & loco-regional recurrence (LRR) (C) in a subset of TCGA patients treated uniformly with surgery and radiation and known patterns of failure. B & C) Kaplan-Meier curves for LRR in patients with either CASP8 (D) or CREBBP/EP300 (E) mutations.

Figure 2. *In vivo* shRNA screening identifies synthetic cytotoxicity CREBBP/EP300 mutated tumors. A) Plot of RSA log p-values from control or irradiated tumors from the *in vivo* shRNA study. Targets below and to the left of the blue dashed line were selected for further examination as potential targets for synthetic cytotoxicity in combination with radiation. B & C) Ratio of CASP8 (B) or CREBBP/EP300 (C) mutant vs. wild type for target fold change (y-axis) and RSA log p-value (x-axis) for targets selected from (A). D & E) Difference between CREBBP/EP300 mutant and wild type tumors from the *in vivo* shRNA study in (C) as a function of target fold change (D) and RSA log p-value (E). F) Clonogenic assays following irradiation of HNSCC cell lines expressing control and either CREBBP or EP300 shRNA. In D & E, comparisons were evaluated using ANOVA with post-hoc Tukey's t-test. In F, each point for each group was compared to control using Student's t-test. For * - shCREBBP-2 and # - shCREBBP-3, $p<0.05$. All p-values two sided.

Figure 3. CBP-p300 coactivator mediated synthetic cytotoxicity results in impaired HR and increased apoptosis. A & B) Tunel staining (A) and caspase 3

immunoblot (B) following irradiation in HNSCC cells expressing control or CREBBP shRNA. (C) γ-H2AX, 53BP1, and BRCA1 foci following irradiation in shControl or shCREBBP HNSCC cells. Significance tested via students t-test. For A, * indicates a two-sided $p<0.05$ compared to the Control XRT group. For B & C two sided p-values are indicated.

Figure 4. CBP-p300 coactivator mediated synthetic cytotoxicity is observed in multiple *in vivo* HNSCC models. A & B) Tumor growth delay (A) and survival (B) in a UM-SCC-47 xenograft model expressing either control or two different CREBBP shRNAs following irradiation at 2 Gy/day for 5 days. C) *In vivo* TUNEL staining from UM-SCC-47 xenograft tumors collected 8h following the final dose of radiation in a concurrent experiment with (A). C) A similar experiment performed in the UM-SCC-22a xenograft model. For both models, the slope of the linear regression for both irradiated CREBBP KD groups was significantly different from other groups with at least a two-sided $p<0.01$. In B, log rank statistics comparing shCREBBP-2 XRT or sh-CREBBP-3 XRT groups compared to Control XRT showed a significant increase in survival (two-sided $p<0.05$) in both groups.

Figure 5. ICG 001 produces synthetic cytotoxicity in CREBBP mutant HNSCC cell lines. A-D) Clonogenic survival following irradiation and ICG-001 in CREBBP mutant (A & B) and wild type (C & D) cell lines. E) Tunel assay following the same combination (p-values are two-sided and derived from Student's t-test). Clonogenic survival curves analyzed as in Figure 2.

Figure 6. The HAT inhibitor A485 exhibits synthetic cytotoxicity in HNSCC cells with mutations in the CBP-p300 co-activator family. A & B) Clonogenic survival

following irradiation and either A485 (active) or A486 (inactive) in CREBBP/EP300 mutant (A) or wild type (B) HNSCC cells. C & D) TUNEL assay (C) and Caspase 3 cleavage (D) in UM-SCC-47 (CREBBP mut), HN5 (CREBBP/EP300 mut) and HN31 (CREBBP/EP300 wt) cells treated with irradiation and either A485 (active) or A486 (inactive). E) iSceI assay for HR as described in the methods following treatment with either A485 or A486. F) Survving fraction at 2 Gy from clonogenic assays following exposure to A485. *,+-<0.05 vs. Control (*) and A486 (+). p-values are two-sided and derived from Student's t-test.

Figure 7. Inhibition of CBP-p300 co-activator family function inhibits acetylation of key histone marks in HNSCC cells that exhibit synthetic cytotoxicity. A-C) Histone acid extraction shows that A-485 (A), shCREBBP (B) and ICG-001 (C) leads to inhibition of H3K18ac and H3K27ac in cell lines that harbor a mutation in CREBBP/EP300.

Figure 8. Potential gain of function mutation in CREBBP mutant cells. A-E) Immunoblot (IB), histone acid extraction or immunoprecipitation (IP) for either CBP, acetyl-lysine or BRCA1 was performed as indicated in the individual panels. A) Cell lines with a CREBBP mutation in the TAZ2 domain have increased global protein acetylation (IP acetyl lysine & IB for acetyl lysine), CBP-auto acetylation (IP CBP & IB for acetyl lysine) and histone acetylation (acid extraction and IB) compared to wild type HNSCC cell lines. B) CBP-auto and histone acetylation are inhibited by A485 in CREBBP mutant lines. C & D) Forced expression of mutant CBP in 293T and HN31 cell lines leads to increased global protein and CBP-auto acetylation (C) as well as histone (D) acetylation (densitometry below blot), compared to forced expression of wild type.

E) Knock out of wild type CBP only (but allowing the expression of the mutant form), in UM-SCC-22a cells led to increased clonogenic survival. An effect that was reversed by forced over expression of wild type CBP. This was not observed in wild type HN31 cells. FL- full length CBP construct, Q1773X – CBP mutant construct, CBP^ - forced expression of full length CBP. *,+-<0.05 vs. Control (*) and CBP KO + CBP^ (+). p-values are two-sided and derived from Student's t-test.

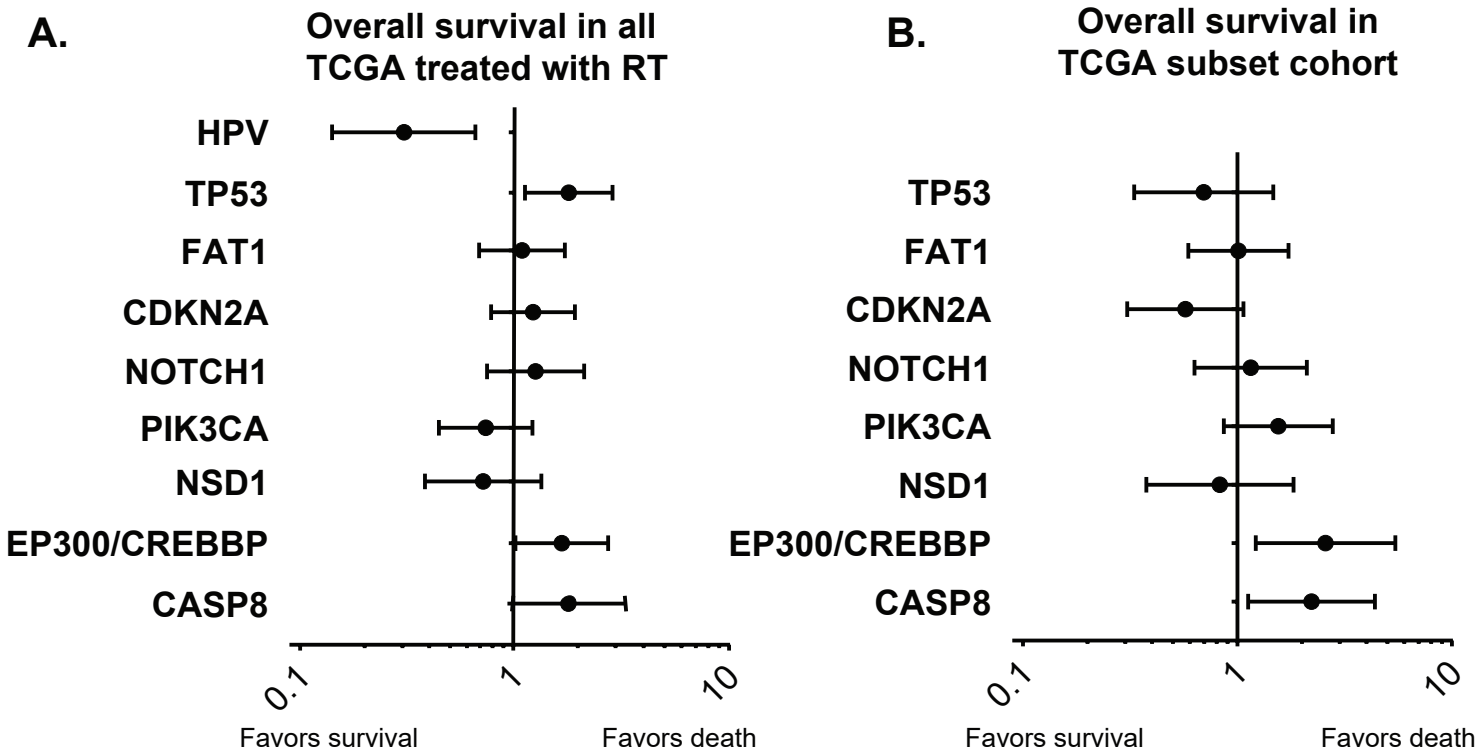

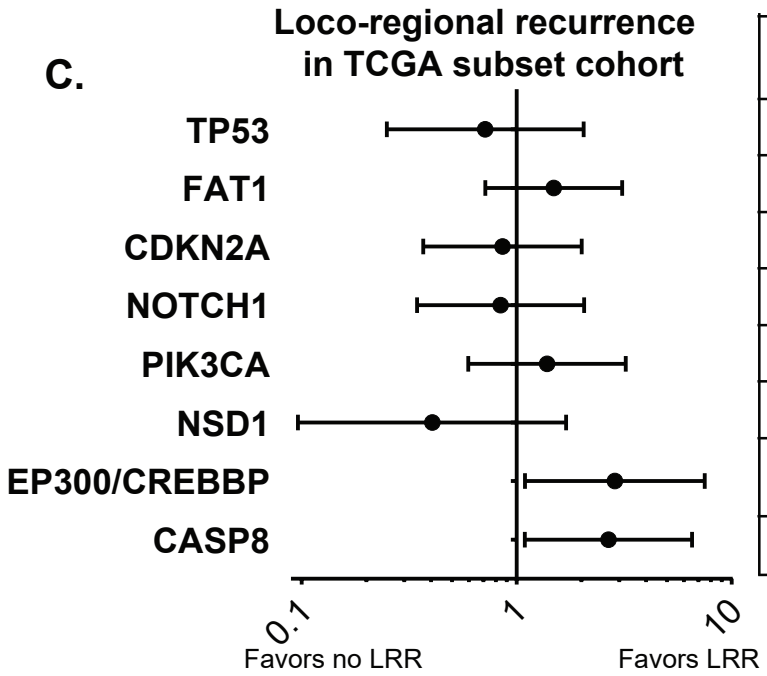

HR	95% CI		p
0.71	0.25	2.05	0.53
1.49	0.72	3.10	0.29
0.86	0.37	2.01	0.73
0.84	0.34	2.06	0.71
1.39	0.60	3.22	0.45
0.41	0.10	1.70	0.22
2.86	1.10	7.50	**0.03**
2.67	1.10	6.54	**0.03**

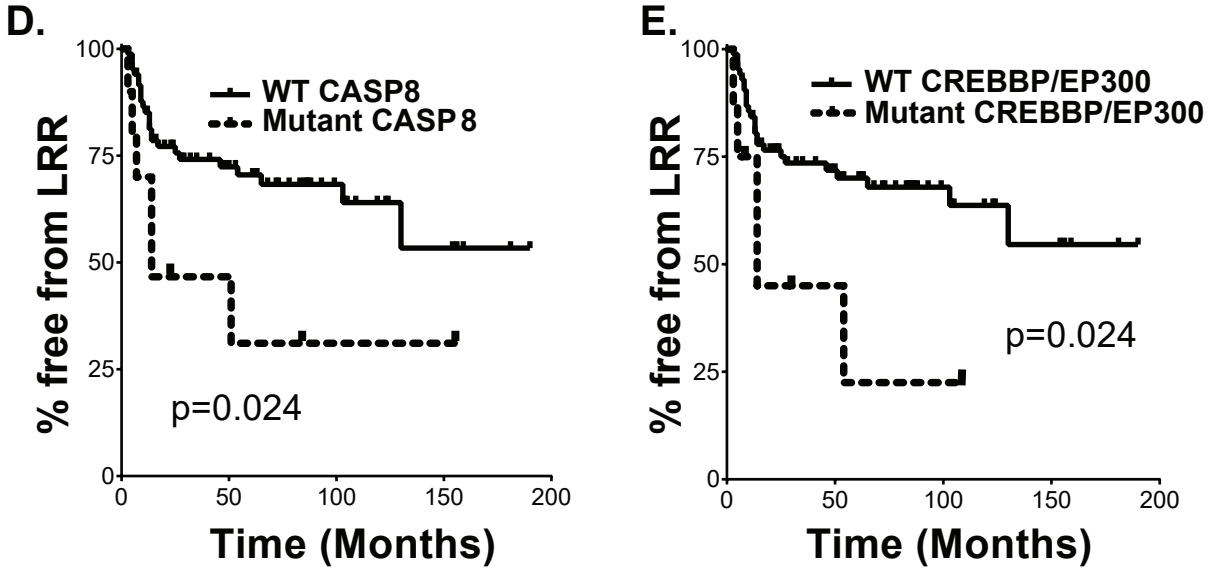

Figure 1

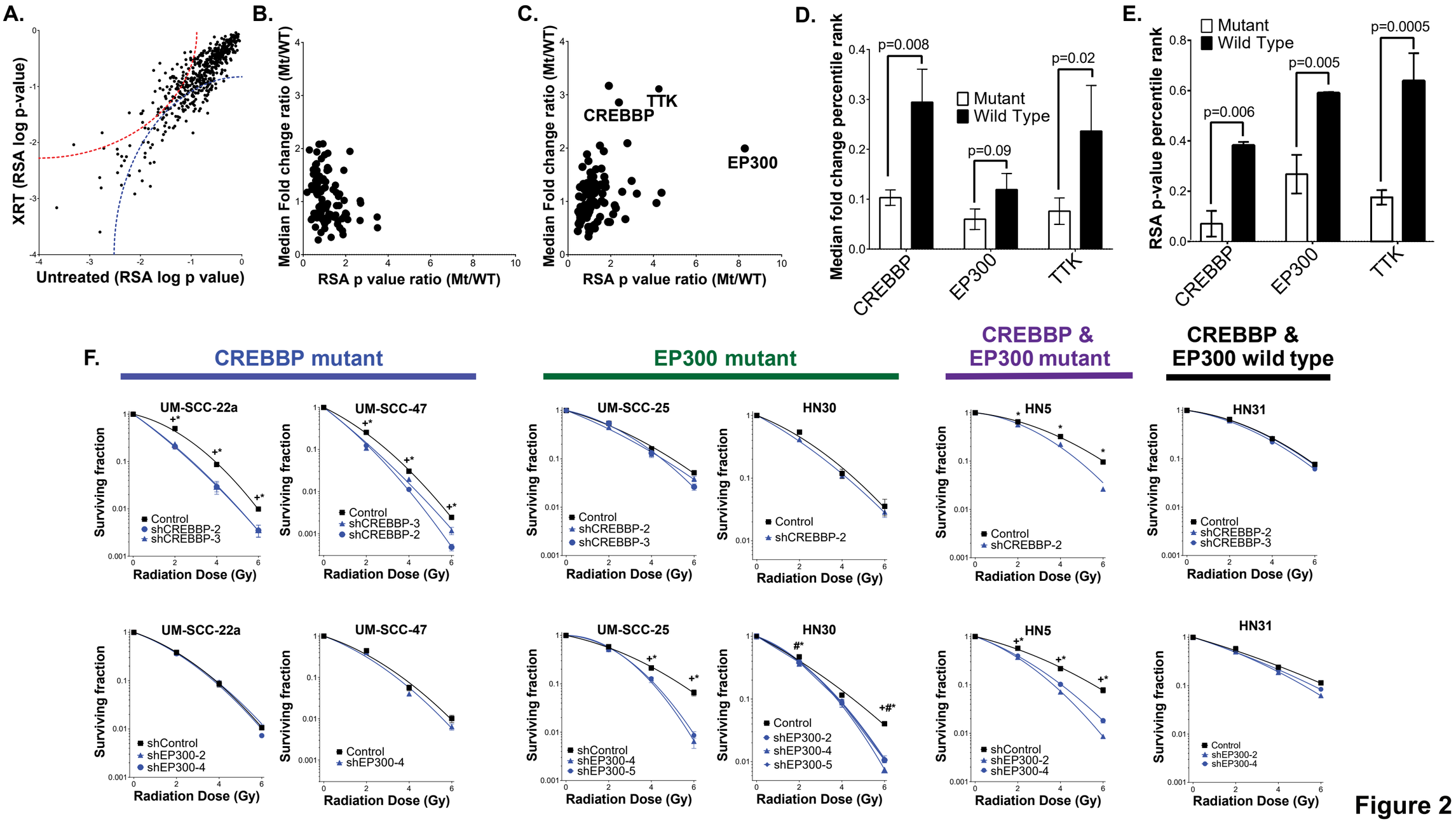
A.
XRT (RSA log p-value)
Untreated (RSA log p value)
B.
Median Fold change ratio (Mt/WT)
RSA p value ratio (Mt/WT)
C.
Median Fold change ratio (Mt/WT)
RSA p value ratio (Mt/WT)
TTK
CREBBP
EP300
D.
Median fold change percentile rank
Mutant
Wild Type
p=0.008
p=0.09
p=0.02
CREBBP
EP300
TTK
E.
RSA p-value percentile rank
Mutant
Wild Type
p=0.006
p=0.005
p=0.0005
CREBBP
EP300
TTK
F.
CREBBP mutant
EP300 mutant
CREBBP & EP300 mutant
CREBBP & EP300 wild type
UM-SCC-22a
UM-SCC-47
UM-SCC-25
HN30
HN5
HN31
Surviving fraction
Radiation Dose (Gy)
Control
shCREBBP-2
shCREBBP-3
shCREBBP-2
shCREBBP-3
shCREBBP-2
shCREBBP-2
shCREBBP-3
shControl
shEP300-2
shEP300-4
Control
shEP300-4
shControl
shEP300-4
shEP300-5
Control
shEP300-2
shEP300-4
shEP300-5
shControl
shEP300-2
shEP300-4
Control
shEP300-2
shEP300-4

Figure 2

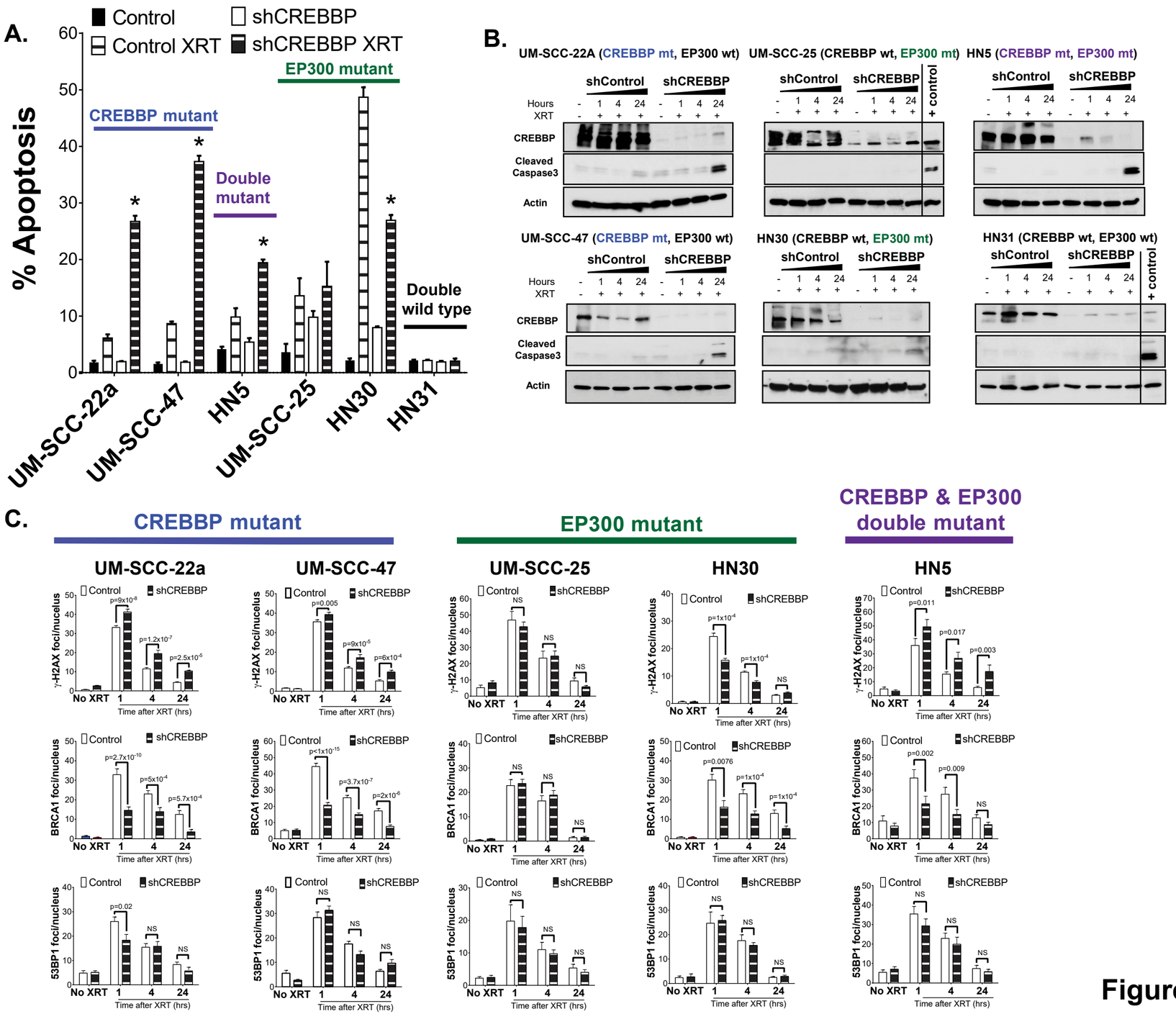
A.
Control
Control XRT
shCREBBP
shCREBBP XRT
% Apoptosis
CREBBP mutant
Double mutant
EP300 mutant
Double wild type
UM-SCC-22a
UM-SCC-47
HN5
UM-SCC-25
HN30
HN31
B.
UM-SCC-22A (CREBBP mt, EP300 wt)
UM-SCC-25 (CREBBP wt, EP300 mt)
HN5 (CREBBP mt, EP300 mt)
UM-SCC-47 (CREBBP mt, EP300 wt)
HN30 (CREBBP wt, EP300 mt)
HN31 (CREBBP wt, EP300 wt)
shControl
shCREBBP
Hours
XRT
CREBBP
Cleaved Caspase3
Actin
+ control
C.
CREBBP mutant
EP300 mutant
CREBBP & EP300 double mutant
UM-SCC-22a
UM-SCC-47
UM-SCC-25
HN30
HN5
γ-H2AX foci/nucleus
BRCA1 foci/nucleus
53BP1 foci/nucleus
Time after XRT (hrs)
No XRT
NS

Figure 3

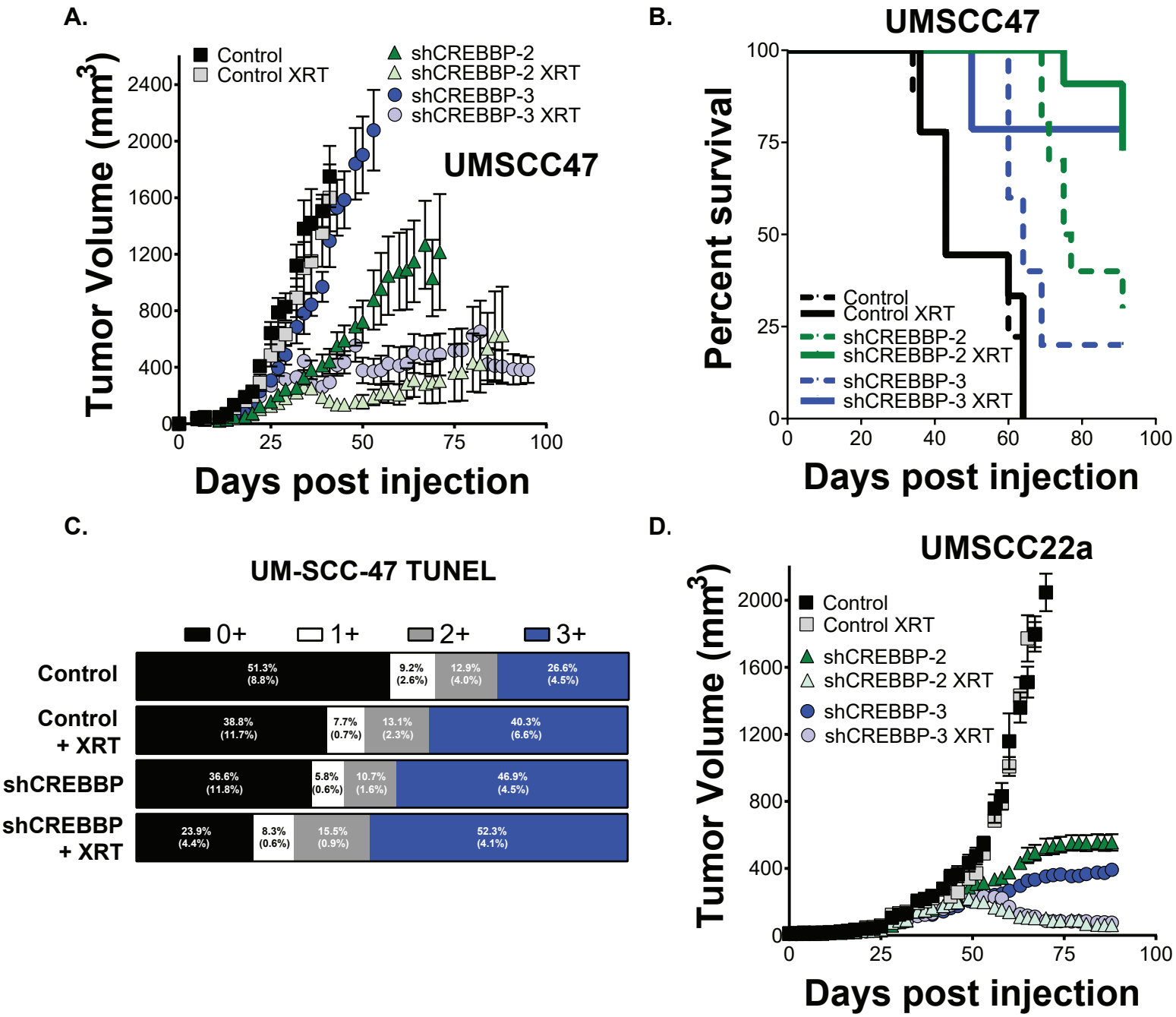
A.
Control
Control XRT
shCREBBP-2
shCREBBP-2 XRT
shCREBBP-3
shCREBBP-3 XRT
UMSCC47
Tumor Volume (mm3)
Days post injection
B.
UMSCC47
Percent survival
Control
Control XRT
shCREBBP-2
shCREBBP-2 XRT
shCREBBP-3
shCREBBP-3 XRT
Days post injection
C.
UM-SCC-47 TUNEL
0+
1+
2+
3+
Control
51.3% (8.8%)
9.2% (2.6%)
12.9% (4.0%)
26.6% (4.5%)
Control + XRT
38.8% (11.7%)
7.7% (0.7%)
13.1% (2.3%)
40.3% (6.6%)
shCREBBP
36.6% (11.8%)
5.8% (0.6%)
10.7% (1.6%)
46.9% (4.5%)
shCREBBP + XRT
23.9% (4.4%)
8.3% (0.6%)
15.5% (0.9%)
52.3% (4.1%)
D.
UMSCC22a
Control
Control XRT
shCREBBP-2
shCREBBP-2 XRT
shCREBBP-3
shCREBBP-3 XRT
Tumor Volume (mm3)
Days post injection

Figure 4

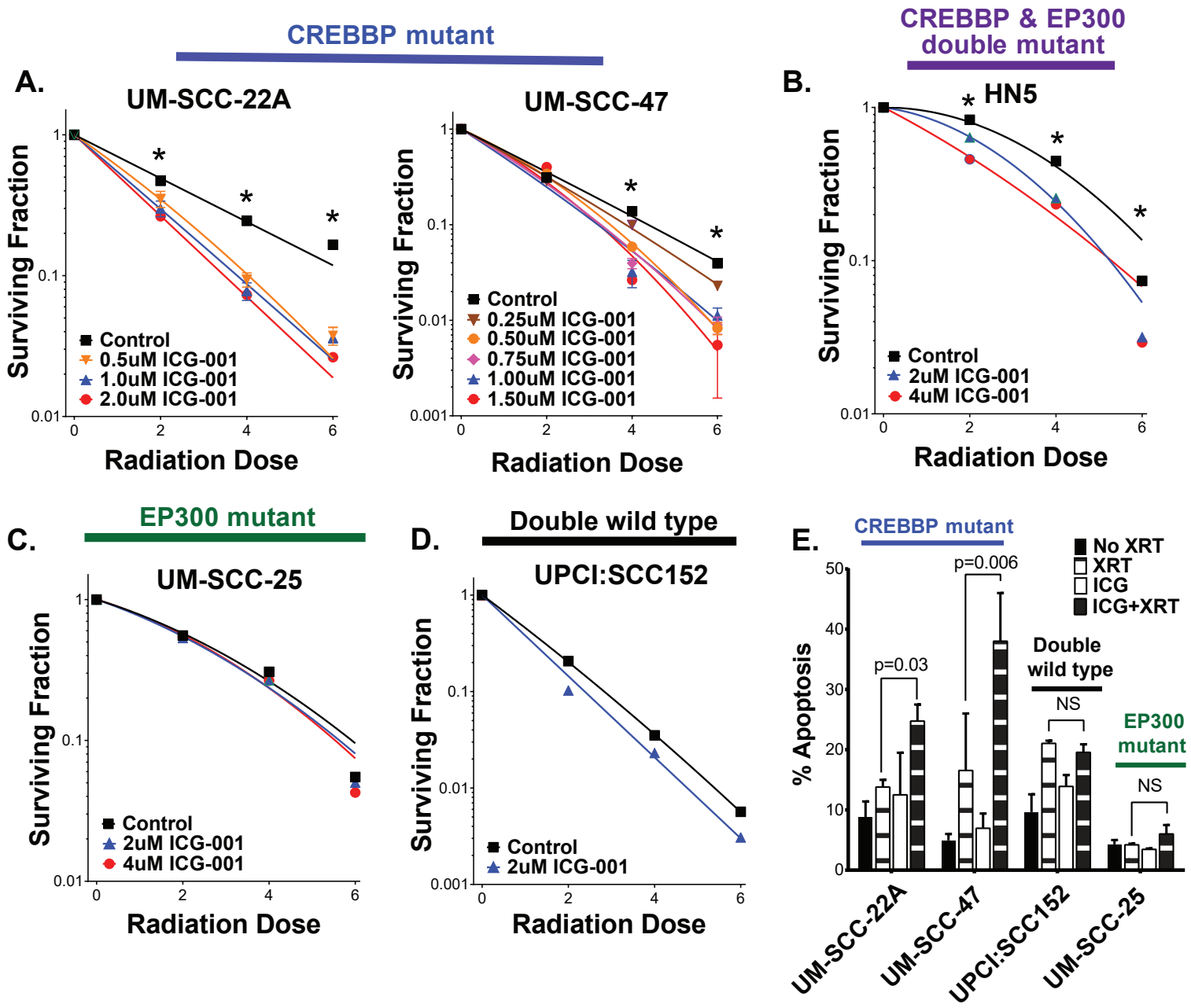
CREBBP mutant
A.
UM-SCC-22A
Surviving Fraction
Radiation Dose
Control
0.5uM ICG-001
1.0uM ICG-001
2.0uM ICG-001
UM-SCC-47
Control
0.25uM ICG-001
0.50uM ICG-001
0.75uM ICG-001
1.00uM ICG-001
1.50uM ICG-001
CREBBP & EP300 double mutant
B.
HN5
Control
2uM ICG-001
4uM ICG-001
EP300 mutant
C.
UM-SCC-25
Control
2uM ICG-001
4uM ICG-001
Double wild type
D.
UPCI:SCC152
Control
2uM ICG-001
E.
CREBBP mutant
No XRT
XRT
ICG
ICG+XRT
% Apoptosis
p=0.03
p=0.006
Double wild type
NS
EP300 mutant
NS
UM-SCC-22A
UM-SCC-47
UPCI:SCC152
UM-SCC-25

Figure 5

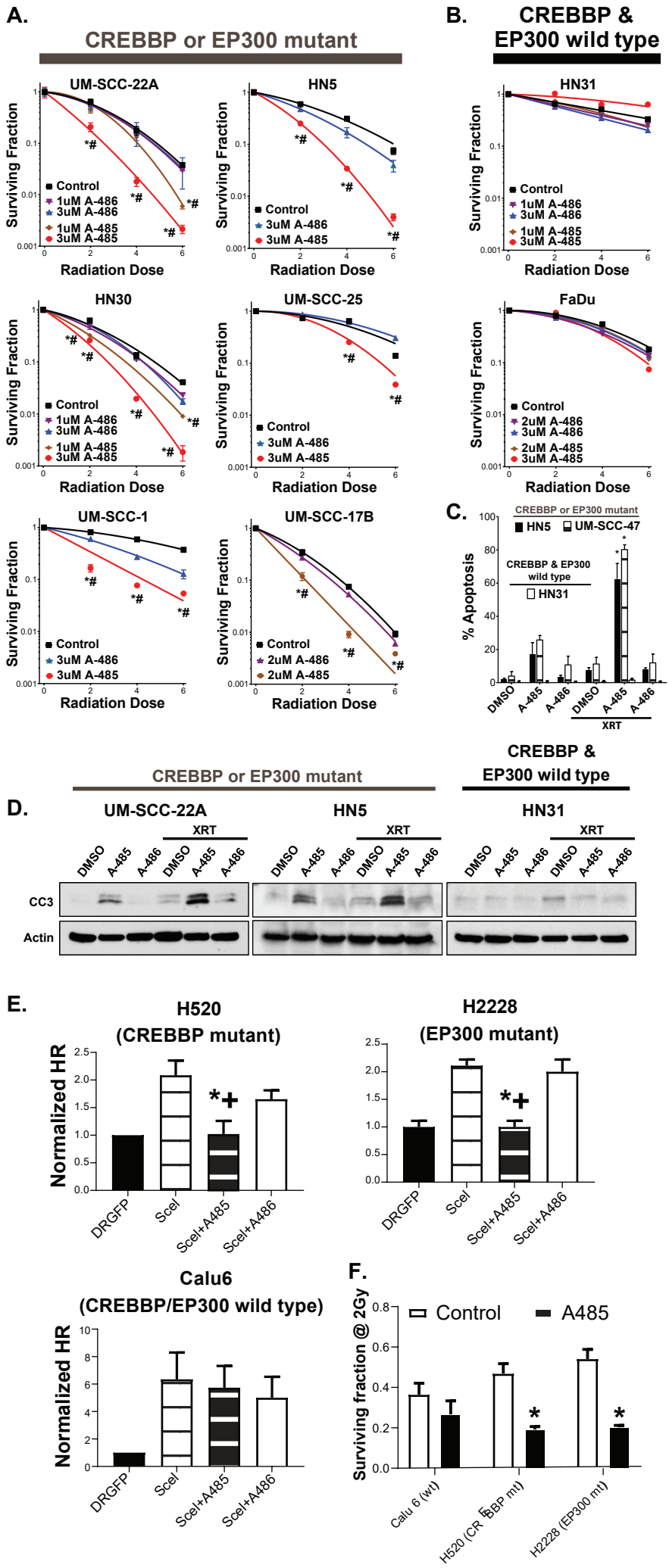
A.
CREBBP or EP300 mutant
B.
CREBBP & EP300 wild type
UM-SCC-22A
HN5
HN31
HN30
UM-SCC-25
FaDu
UM-SCC-1
UM-SCC-17B
Surviving Fraction
Radiation Dose
Control
1uM A-486
3uM A-486
1uM A-485
3uM A-485
2uM A-486
2uM A-485
C.
CREBBP or EP300 mutant
HN5
UM-SCC-47
CREBBP & EP300 wild type
HN31
% Apoptosis
DMSO
A-485
A-486
XRT
D.
CREBBP or EP300 mutant
CREBBP & EP300 wild type
UM-SCC-22A
HN5
HN31
XRT
DMSO
A-485
A-486
CC3
Actin
E.
H520 (CREBBP mutant)
H2228 (EP300 mutant)
Calu6 (CREBBP/EP300 wild type)
Normalized HR
DRGFP
SceI
SceI+A485
SceI+A486
F.
Control
A485
Surviving fraction @ 2Gy
Calu 6 (wt)
H520 (CREBBP mt)
H2228 (EP300 mt)

Figure 6

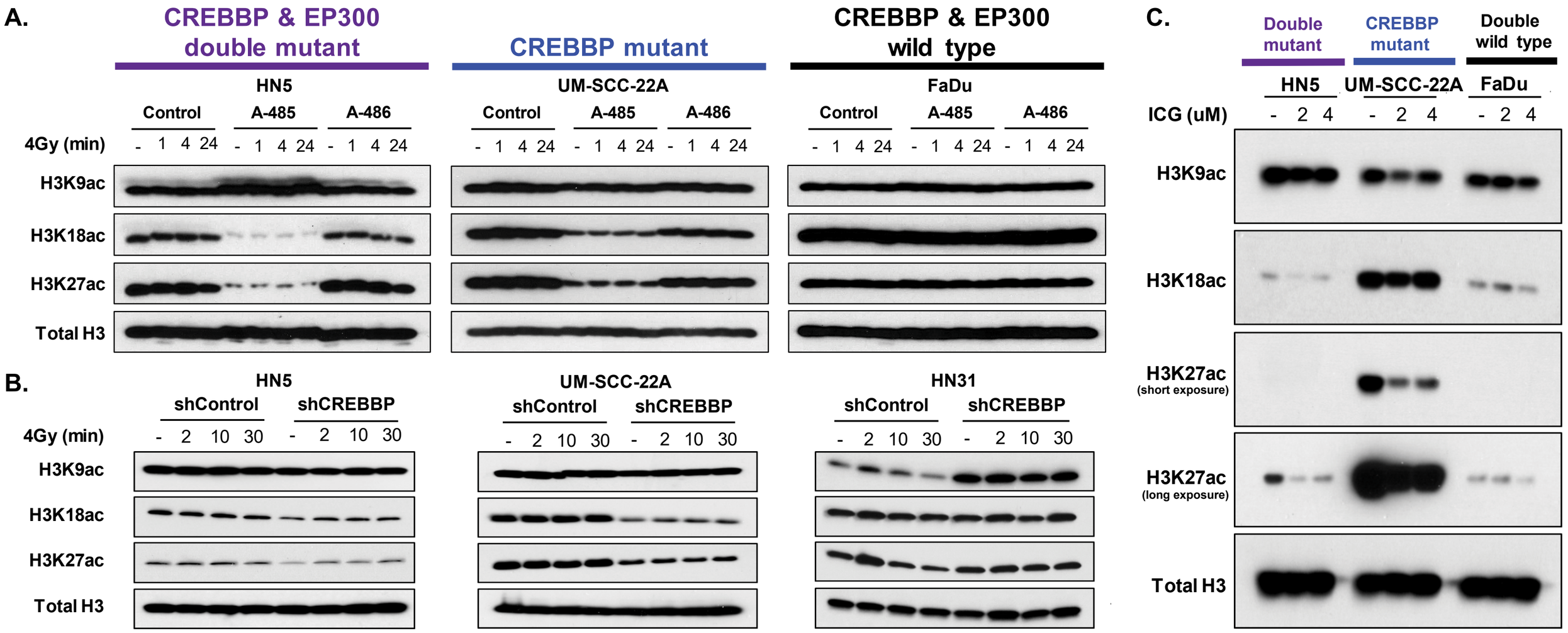
A.
CREBBP & EP300 double mutant
CREBBP mutant
CREBBP & EP300 wild type
HN5
UM-SCC-22A
FaDu
Control
A-485
A-486
4Gy (min)
- 1 4 24
H3K9ac
H3K18ac
H3K27ac
Total H3
B.
HN5
UM-SCC-22A
HN31
shControl
shCREBBP
- 2 10 30
C.
Double mutant
CREBBP mutant
Double wild type
ICG (uM)
- 2 4
H3K27ac (short exposure)
H3K27ac (long exposure)

Figure 7

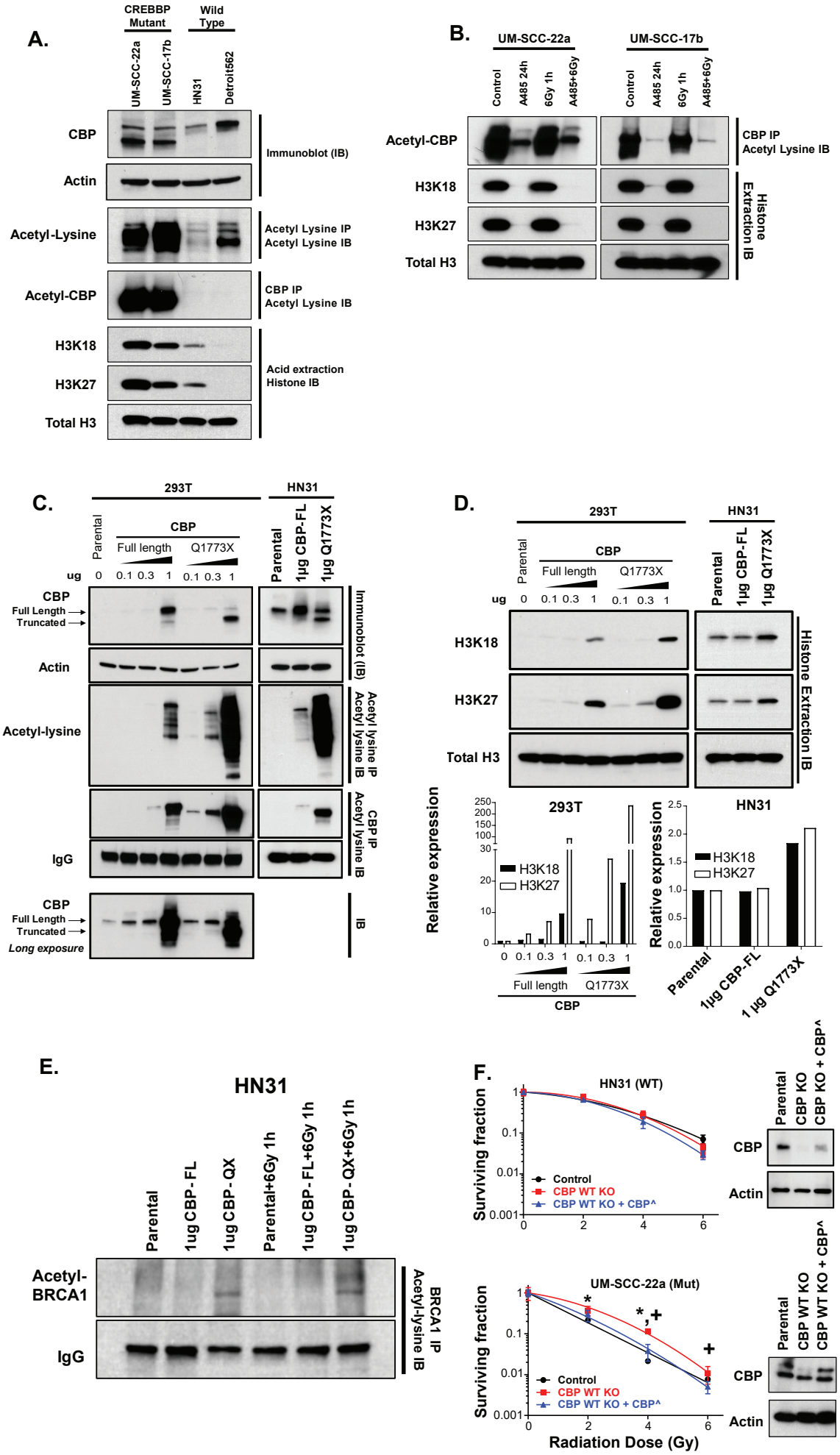
A.
CREBBP Mutant
Wild Type
UM-SCC-22a
UM-SCC-17b
HN31
Detroit562
CBP
Actin
Immunoblot (IB)
Acetyl-Lysine
Acetyl Lysine IP
Acetyl Lysine IB
Acetyl-CBP
CBP IP
Acetyl Lysine IB
H3K18
H3K27
Total H3
Acid extraction
Histone IB
B.
UM-SCC-22a
UM-SCC-17b
Control
A485 24h
6Gy 1h
A485+6Gy
Acetyl-CBP
CBP IP
Acetyl Lysine IB
H3K18
H3K27
Total H3
Histone Extraction IB
C.
293T
HN31
Parental
CBP
Full length
Q1773X
ug
0 0.1 0.3 1 0.1 0.3 1
1µg CBP-FL
1µg Q1773X
CBP
Full Length
Truncated
Actin
Immunoblot (IB)
Acetyl-lysine
Acetyl lysine IP
Acetyl lysine IB
IgG
CBP IP
Acetyl lysine IB
Long exposure
IB
D.
293T
HN31
Parental
CBP
Full length
Q1773X
ug
0 0.1 0.3 1 0.1 0.3 1
1µg CBP-FL
1µg Q1773X
H3K18
H3K27
Total H3
Histone Extraction IB
Relative expression
293T
HN31
H3K18
H3K27
Full length
Q1773X
CBP
Parental
1µg CBP-FL
1 µg Q1773X
E.
HN31
Parental
1ug CBP-FL
1ug CBP-QX
Parental+6Gy 1h
1ug CBP-FL+6Gy 1h
1ug CBP-QX+6Gy 1h
Acetyl-BRCA1
IgG
BRCA1 IP
Acetyl-lysine IB
F.
HN31 (WT)
Surviving fraction
Control
CBP WT KO
CBP WT KO + CBP^
Parental
CBP KO
CBP KO + CBP^
CBP
Actin
UM-SCC-22a (Mut)
Radiation Dose (Gy)

Figure 8